Molecular Dynamics Simulations of Water Structure and Diffusion in Silica Nanopores

Ian C. Bourg[*] *& Carl I. Steefel*

Geochemistry Department, Earth Sciences Division, Lawrence Berkeley National Laboratory, Berkeley CA 94720

* icbourg@lbl.gov

ABSTRACT

We present molecular dynamics (MD) simulations of water-filled silica nanopores such as those that occur in ordered oxide ceramics (MCM-41, SBA-15), controlled pore glasses (such as Vycor glass), mesoporous silica, bioglasses, and hydrous silica gel coatings of weathered minerals and glasses. Our simulations overlap the range of pore diameters (1 to 4 nm) where confinement causes the disappearance of bulk-liquid-like water. In ≥ 2 nm diameter pores, the silica surface carries three statistical monolayers of density-layered water, interfacial water structure is independent of confinement or surface curvature, and bulk-liquid-like water exists at the center of the pore (this last finding contradicts assumptions used in most previous neutron diffraction studies and in several MD simulation studies of silica nanopores). In 1 nm diameter pores, bulk-liquid-like water does not exist and the structural properties of interfacial water are influenced by confinement. Predicted water diffusion coefficients in 1 to 4 nm diameter pores agree with quasi-elastic neutron scattering (QENS) data and are roughly consistent with a very simple "core-shell" conceptual model whereupon the first statistical water monolayer is immobile and the rest of the pore water diffuses as rapidly as bulk liquid water.

KEYWORDS: Nanopore, confined water, molecular dynamics simulation, silica, surface water, diffusion.

INTRODUCTION

How do the properties of water confined in hydrophilic silica nanopores differ from those of bulk liquid water? This fundamental question has implications for the utility of synthetic nanoporous silicates such as ordered oxide ceramics (MCM-41, SBA-15)[1-3], controlled pore glasses (CPG, including Vycor glass)[1,4], mesoporous silica[5,6], and bioglasses[7]. In geochemistry, it determines the influence of hydrous silica gel coatings on the long-term weathering rates of silicate glasses and minerals[8,9], these rates being important unknowns in studies of soil formation[10] and global carbon cycling[11] and in predicting the fate of CO_2[12,13] and high-level radioactive waste in geological repositories[14,15]. From a theoretical perspective, the question is compelling because hydrophilic silica nanopores can be readily fabricated with well-controlled structural features (the materials listed above have an amorphous SiO_2 matrix, silanol surface functional groups, cylindrical pores, and pore diameters that can be varied from about 1 nm to more than 100 nm[1-4,6]) for probing the new physics of water that occur due to finite-size effects, a frontier research area with broad implications in catalysis[16], biology[17,18], nanofluidics[19,10], membrane science[2`], and the geosciences[21-23].

Theoretical models of transport and chemistry in water-filled nanopores routinely rely on the simplifying approximation that water properties are not modified by confinement[19], but this approximation is expected to fail in nanoporous media where pore size approaches the diameter of a water molecule[20]. Studies of water in hydrophilic nanopores carried out with a range of techniques (thermoporometry[1,24], capillary imbibition[25], surface force apparatus[22,26], infrared and Raman spectroscopy[4,17,18,21,27], NMR spectroscopy[28], X-ray and neutron diffraction[6,29-31], quasi-elastic neutron

scattering[2,32], molecular dynamics simulations[26,33-36]) show that this failure occurs in pores narrower than ~20 nm and can be classified into two regimes. The first regime occurs in pores that are about 2 to 20 nm wide and results from "surface water" [water with structure and dynamics distinct from those of bulk liquid water, found within up to three statistical monolayers (~0.9 nm) from hydrophilic surfaces[34,35]] constituting a non-negligible part of the pore water[25,27,34]. In this regime, the average behavior of pore water is sometimes represented with a "core-shell" model, on which pore water is conceptually divided into a core of "free" water with bulk-liquid-like properties and a shell of "surface" water with distinct properties[25,27]. The second regime occurs in pores that are narrower than about 2 nm, where the bulk-liquid-like water core is absent[2,34] and surface water is influenced by confinement between two surfaces rather than by interaction with a single surface[26]. In this second regime, the average properties of water in hydrophilic nanopores are poorly understood, highly sensitive to pore size and surface properties, and may diverge strongly from those of bulk liquid water[18,23,26,33].

Early research on the physics of water in water-filled cylindrical hydroxylated silica nanopores focused substantially on the low-temperature phase transitions of confined water[1,24,28,29]. These studies showed that in 2 to 12 nm diameter pores, a 0.4 to 0.6 nm-thick surface water layer freezes at a much lower temperature than the free pore water and does not form a crystalline ice phase[24,28,29]. Ice crystals formed in the free pore water in 2.4 nm diameter pores have a smaller lattice constant than those formed in 4.2 nm diameter pores, suggesting that confinement influences the structure of water even in the core region[29]. More recent research has concentrated on revealing the properties of ambient liquid water in silica nanopores including its structure[3,6,31], vibrational

dynamics[4], diffusivity[2,32], and viscosity[25]. These studies showed that the first one or two statistical water monolayers on the silica surface are ordered and much less mobile than the rest of the pore water[3,25,37]. However, contradictory results have been reported on the influence of confinement on water density[3,37] and hydrogen bond structure[4,31] beyond the first two surface water layers. Furthermore, very few studies[2] have probed the molecular-scale properties of liquid water in silica nanopores for a range of pore diameters overlapping the expected transition between the first and second confinement regimes.

Molecular dynamics (MD) and Monte Carlo (MC) simulations are well suited for revealing the structure and dynamics of water in nanopores[34-36]. However, of the MD and MC simulation studies that have probed water in silica nanopores[33,37-45], only four studies used an amorphous SiO_2 structure, silanol surface functional groups, and water-filled cylindrical nanopores[37,38,40,43]. Gallo et al.[38] simulated a 4 nm diameter pore, but they focused on conditions where the pore was either filled with supercooled water or partially filled. Leung et al.[40] simulated a 1.2 nm diameter pore using Grand Canonical Monte Carlo (GCMC) and *ab initio* MD simulations, but they did not characterize the pore water structure and they simulated time and length scales much too short to accurately probe water diffusion (4.5 ps, < 400 atoms). Recently, Lerbret et al.[37] carried out 4 ns MD simulations of a 3 nm diameter pore with two different densities of silanol functional groups, and Milischuk and Ladanyi[43] carried out 2 ns MD simulations of 2, 3, and 4 nm diameter pores with a low density of silanol functional groups. Here, we present the results of MD simulations of water-filled cylindrical hydroxylated silica nanopores that differ from previous simulations in several important aspects. Firstly, we probe a range of pore diameters (1, 2, and 4 nm) that overlaps the transition between the first and

second confinement regimes. Secondly, our simulated nanopores connect two bulk liquid water reservoirs. This ensures that our pores are fully water-filled, and it allows us to observe diffusion through the pores. Finally, we probe time and length scales larger than in previous studies (7 to 62 ns simulations; 16,041 to 63,321 atoms per simulation cell). We determine for the first time the influence of confinement on the structure and diffusion coefficient of liquid water in this type of nanopore for a range of pore diameters.

METHODOLOGY

Details of our simulations are described in the Electronic Annex. Briefly, our simulated systems consisted of a 6-nm-thick SiO_2 glass slab pierced by a cylindrical nanopore with a diameter of 1, 2, or 4 nm. Under-coordinated surface O and Si atoms were "healed" with H or OH groups as in previous studies[38,40]. The density of silanol groups, 6.6 ± 0.2 sites per nm^2, was lower than the values predicted with other inter-atomic potential models (6.8 to 7.6 sites per nm^2)[37,40,46] and higher than that measured for silica surfaces (4.9 ± 0.5 sites per nm^2)[47]. As pointed out by Leung et al.[40], the apparent discrepancy between experimental and predicted site densities may derive from a difference in the definition of surface area: our calculations used an "ideal" surface area derived as if our solid were a smooth slab pierced by a smooth cylindrical pore, whereas Zhuravlev[47] used the "effective" surface area probed by low temperature adsorption of Kr. The effective surface area must be greater than the ideal surface area because Kr atoms probe the atomistic-scale roughness of the amorphous silica surface. The MD simulation methodologies used by Gallo et al.[38] and Millischuk and Ladanyi[43] yielded

much lower site densities (2.0 to 2.5 sites per nm^2). Sufficient water molecules were added to each simulation cell to fill the nanopore and to form a 4-nm-thick water film on both sides of the glass slab (Fig. 1). The 1 and 2 nm diameter pore systems had simulation cell dimensions of $31.65 \times 36.54 \times 190.0$ $Å^3$ (16,794 and 16,041 atoms, respectively); the 4 nm diameter pore system was twice as large in the *x* and *y* dimensions ($63.29 \times 73.08 \times 190.0$ $Å^3$, 63,321 atoms). The 1, 2, and 4 nm diameter pore systems were simulated for durations sufficiently long to observe steady-state water diffusion through each pore (62, 23, and 7 ns, respectively, following 3 ns of equilibration at 298 K). Unless otherwise specified, simulations were carried out in the *NVT* ensemble with a 0.5 fs time step, long-range (> 15.0 Å) Coulomb and van der Waals interactions were treated by Ewald summation with 99.99% accuracy, and temperature was controlled using a Nosé-Hoover thermostat with a coupling constant of 100 ps. Simulations were carried out with the code LAMMPS[48] and visualized with the code VMD[49].

Molecular dynamics simulations of silica-water systems are sensitive to the choice of interatomic potential models, the main input of these simulations[39,41,50]. To our knowledge, at least 15 models have been used to describe inter-atomic interactions in MD simulations of bulk liquid water in contact with hydroxylated silica surfaces[37-41,51-60]. Prior to our silica nanopore simulations, we selected silica-water interatomic potential models that comprised only two-body interactions (for later use with well-tested models of aqueous solutes and non-aqueous fluids) and that included short-range and Coulombic interaction parameters for Si, O, hydroxyl O (denoted as Oh), and H atoms[39,40,51,55] (see Table A1 in the electronic annex). We tested these models against experimental data on the density profile of water on the $10\bar{1}0$ surface of α-quartz[62] (the four models

performed similarly; see Table 2 in the Electronic Annex) and on the structure of SiO_2 glass[61] (the CLAYFF model of Cygan et al.[55] gave a much more accurate prediction as shown in Table 1). Skelton et al.[50] recently found that CLAYFF is consistent with *ab initio* MD predictions of water structure on the $10\bar{1}1$ quartz surface. On the basis of our test simulations and the results of Skelton et al.[50], we adopted the CLAYFF model in combination with the extended simple point charge (SPC/E) water model[64] for simulating water in silica nanopores. This combination of models is known to accurately predict the structure, diffusion coefficient (in systems of a few hundred water molecules), and static dielectric constant of ambient liquid water[65-67] and the behavior of water in clay interlayer nanopores[23,68,69].

RESULTS

Water density distribution. Maps of the average density of water O and H atoms (ρ_{Ow}, ρ_{Hw}) indicate that water is strongly structured by the silica surface (Fig. 2). The location of the Gibbs surface of water (calculated from ρ_{Ow} as described in the Electronic Annex, identified hereafter with the silica-water interface) shows that the simulated silica slab has an effective thickness of 61.4 ± 0.2 Å (average value for the three simulated systems, with error calculated as two standard deviations) and that the 1, 2, and 4 nm diameter pores have effective radii of 4.37, 9.37, and 19.49 Å. Plots of ρ_{Ow} and ρ_{Hw} vs. distance from flat or curved silica surfaces (Fig. 3) reveal density layering extending up to about 9 Å (three statistical water monolayers) from the silica surface, in agreement with water density layering observed in experimental and MD simulation studies of water near other solid surfaces[35,62,70]. The water layers are more pronounced in Fig. 2 than in

Fig. 3, because the latter figure reports ρ_{Ow} values that are "smoothed out" by averaging over a greater area of the rough silica surface (ρ_{Ow} values in Fig. 2 are averaged over the circumference of the pore; values in Fig. 3 are additionally averaged over the length of the pore). The density profile shoulder at $z \sim -1$ Å is produced by water molecules that become ensconced in small "pockets" of the amorphous silica surface[37,38]. The slope leading up to the $\rho_{Ow}(r)$ peak at 2.0 ± 0.1 Å is less steep than on smooth surfaces[35] in accord with the measured ~ 2 Å roughness of MCM-41 silica pore walls[3].

Water density at the center of our silica nanopores reveals that the transition between the first and second confinement regimes (discussed in the Introduction) occurs at a pore diameter between 1 and 2 nm, in agreement with previous studies[2]. Water density is bulk-liquid-like at the center of ≥ 2 nm diameter pores but shows strong oscillations at the center of the 1 nm diameter pore. Our finding of a bulk-liquid-like water density at the center of ≥ 2 nm diameter pores is consistent with studies of other nanoporous media[34-36] but it contradicts several neutron diffraction studies[3,31] and at least one MD simulation study[38] that assumed that the average density of water in silica nanopores is 11 % lower than that of bulk liquid water. This assumption was based on a single paper[71] where we found no mention of a low density of water in silica nanopores. Recently, grand canonical Monte Carlo (GCMC) simulations predicted that water density at the center of 2 to 4 nm diameter silica nanopores is about 10 % lower than in bulk liquid water[43], whereas a MD simulation of a 3 nm diameter pore equilibrated with bulk liquid water yielded results consistent with our findings[37].

Water density near the pore surface (Fig. 3 at $d < 4$ Å) shows that the disappearance of bulk-liquid-like pore water at diameters between 2 and 1 nm coincides with a

significant distortion of the first statistical water monolayer on the silica surface. In the 2 and 4 nm diameter pores, ρ_{Ow} profiles near the curved silica surface are essentially identical to the profile on flat surfaces (Fig. 3b). In the smallest pore, where bulk-liquid-like water does not exist, water O atom density is significantly enhanced near the silica surface (Fig. 3b). We hypothesize that this enhancement results from steric effects that prevent optimal water-water hydrogen bonding inside the pore. As noted in the Introduction, previous studies indicate the existence of a transition in confinement regime at pore widths near 2 nm. Our prediction of a strong distortion of interfacial water structure at pore widths below 2 nm is consistent with this transition.

We note in passing that the density profiles of water H atoms in 2 and 4 nm diameter pores differ mildly from their profile on flat silica surfaces (Fig. 3c). Since ρ_{Ow} curves on these surfaces are nearly identical, this result suggests that confinement (or curvature) may influence the orientation of interfacial water molecules even at pore diameters above 2 nm. However, the absence of a clear trend in ρ_{Hw} as a function of pore diameter prevents any clear conclusion on the significance of this effect.

Intrinsic proton affinity of silica-water interfaces. One important property of silica nanopores that may be influenced by confinement is the acid-base reactivity of silanol functional groups:

$$>SiOH \Leftrightarrow >SiO^- + H^+. \qquad (1)$$

The reaction described by Eq. (1) determines silica surface charge, an important parameter in the reactivity of silicate glasses and minerals[7,11,72,73] and the design of nanofluidic devices[74,75]. According to bond valence models[76-79], the intrinsic pK_a value of silanol groups may be sensitive to the number of hydrogen bonds received by the

silanol O atom. Therefore, if confinement influences the structure of surface water in silica nanopores, it also could influence the acidity of silanol groups. Indeed, several studies suggest that silanol groups located in silica nanopores have a different acidity than those located on flat silica surface[5,80,81]. To investigate this hypothesis, we used our simulation results to calculate the amount of "bond valence" ($s_{\text{H-bond}}$) received by each silanol O atom (Oh) from H atoms in neighbor silanol groups or water molecules. To evaluate $s_{\text{H-bond}}$ for each Oh atom in our simulations, we calculated the radial distribution functions $g_{\text{OhH}}(r)$ of neighbor silanol or water H atoms around each Oh atom. Then, for each Oh atom, we applied the relationship between hydrogen bond length ($r_{\text{H-bond}}$) and bond valence proposed by Machesky et al.[78]:

$$s_{\text{H-bond}} = \int_{r=1.4\text{Å}}^{r=2.4\text{Å}} (1.55 - 1.06r + 0.186r^2) g_{\text{OhH}}(r) \mathrm{d}r \,. \qquad (2)$$

The cumulative distributions of $s_{\text{H-bond}}$ values of silanol groups located on flat silica surfaces and on the curved surfaces of 1, 2, or 4 nm diameter nanopores are plotted in Fig. 4. Our calculations show that Oh atoms located in silica nanopores receive slightly less bond valence from hydrogen bonds than Oh atoms located on flat silica surfaces (Fig. 4). According to the widely used multi-site complexation (MUSIC) model[76], a 0.05 difference in bond valence translates to approximately a unit difference in the intrinsic pK_a values of protonation reactions. If a similar relationship exists for deprotonation reactions, the average intrinsic pK_a value of silanol sites in silica nanopores should be about 0.5 pH units higher than on flat silica surfaces. This difference is smaller than the precision of reported silanol group pK_a values (7.0 ± 0.6)[73,82,83]. Evidently, water hydrogen bond donation to surface O atoms is essentially insensitive to pore diameter even in the 1 nm diameter pore.

We note that the acidity of silanol groups may depend not only on hydrogen bonding to surface O atoms, but also on the electrostatic screening of charged >SiO$^-$ sites by ions in the electrical double layer[11] and on the dielectric screening of those sites by interfacial water[77,81,84], both of which may vary with confinement or interfacial curvature. Examination of these effects may require using molecular simulation methods that allow proton transfer reactions, such as *ab initio* MD simulations[81,85] or classical MD simulations with so-called "reactive" force fields[58].

Water diffusion in silica nanopores. Water diffusion in silica nanopores was probed at the pore scale by "tagging" water O atoms according to the bulk water reservoir in which they were last located. Water molecules initially located inside the pore ($64.3 < z < 125.7$ Å) were left untagged until they entered one of the bulk water reservoirs. Examples of density profiles of tagged O atoms in the 2 nm diameter pore are shown in the upper part of Fig. 5. Cumulative breakthrough fluxes of water O atoms diffusing through the 1, 2, and 4 nm diameter pores are shown in the lower part of Fig. 5. Our results indicate that simulation times greater than at least 40, 10, and 5 ns are required to observe steady-state water diffusion through the 1, 2, and 4 nm diameter pores, respectively. Steady-state tracer concentration profiles across the pores are essentially linear, indicating that the diffusion coefficient of water is invariant with z. In particular, this means that water molecules exchange freely between the nanopores and the bulk liquid water reservoirs, in agreement with MD simulation studies of clay interlayer nanopores[86,87], but in contradiction with the extant "Renkin model" of diffusion in nanopores[88-91]. Steady-state breakthrough fluxes were calculated from the data in Fig. 5 with the standard expression:

$$D_{\text{nanopore}} = -J / (\Delta C/\Delta z), \quad (3)$$

where J is the steady-state flux (mol m^{-2}) calculated from the long-time slope of the curves in the lower part of Fig. 5 (t > 50, 10, or 5 ns for the 1, 2, and 4 nm diameter pores) and $\Delta C/\Delta z$ is the concentration gradient of tagged water O atoms across the pore (ΔC = 55.3 mol dm^{-3}; Δz = 6.14 ± 0.02 nm). Our calculations yield pore-scale water diffusion coefficients D_{nanopore} = 0.28 ± 0.09, 1.01 ± 0.05, and 1.54 ± 0.13 × 10^{-9} m^2 s^{-1} in the 1, 2, and 4 nm diameter pores.

To gain further insight into the diffusion of water in silica nanopores, we calculated the molecular-scale diffusion coefficient D of water molecules as a function of their (r,z) coordinates using the well known Einstein relation:

$$D = \frac{1}{2n} \lim_{\tau \to \infty} \frac{d\text{MSD}(\tau)}{d\tau}, \quad (4)$$

where MSD(τ) is the mean-square displacement of a diffusing molecular averaged over all molecules of interest and all time intervals of length τ, and n is the dimensionality of the system in which diffusion occurs. In heterogeneous systems such as our simulation cells, application of Eq. 4 is non-trivial because D varies with the location of the diffusing particle. In such systems, use of Eq. 4 requires the existence of an observation time scale τ sufficiently long that particle motion is in the diffusive regime, yet sufficiently short that individual particles do not probe regions with very different D values[35]. On the basis of previous studies[34,35], we approximated Eq. 4 by calculating the slope of MSD(τ) from τ = 2 to 10 ps and by using a MSD(τ) function calculated either in the xy plane or in the z direction, whichever was parallel to the nearest surface. To determine "local" D values, we divided our simulation cell into 0.2-Å-wide regions in the r and z dimensions; for each of these regions, we calculated a MSD(τ) function using all

10 ps water O atom trajectories that started in this region. Calculated $D(r,z)$ values are mapped in the three simulated systems in Fig. 6 and plotted as a function of distance from the silica surface in Fig. 7. Figure 6 shows that water diffuses more rapidly near the liquid-vapor interface, in agreement with previous studies[92]. The predicted D value of water far from any interface ($D = 3.16 \pm 0.19 \times 10^{-9}$ m^2 s^{-1}, average value calculated in the region where z = 36 to 40 or 150 to 154 Å in our three simulations) is consistent with previous studies of the self-diffusion coefficient of bulk liquid SPC/E water ($D_0 = 2.4 \pm 0.4 \times 10^{-9}$ m^2 s^{-1} in simulations of 216 water molecules[65], increasing with the size of the simulation cell—a well known artifact of MD simulations[93]—to an extrapolated value of $D_0 = 2.84 \times 10^{-9}$ m^2 s^{-1} in infinitely large systems[94]; for comparison, $D_0 = 2.299 \times 10^{-9}$ m^2 s^{-1} for real liquid water at 298 K[95]) and with studies showing that in asymmetric simulation cells, MD simulations predict larger water diffusion coefficients in directions along which the simulation cell is shorter[36]. The density-weighted average value of D in our silica nanopores (calculated for z = 75 to 115 Å) yields $D_{\text{nanopore}} = 0.17 \pm 0.04$, 1.06 ± 0.04, and $1.82 \pm 0.01 \times 10^{-9}$ m^2 s^{-1} in the 1, 2, and 4 nm diameter pores (confidence intervals were calculated as two standard errors of the mean using four 10 Å segments of each nanopore). The good agreement between the D_{nanopore} values calculated at the molecular scale (this paragraph) and at the pore scale (previous paragraph) shows that the two methods are essentially equivalent even though they probe very different time scales (ten picoseconds vs. nanoseconds, respectively).

Our predicted D_{nanopore} values are compared in Figure 8 with experimental results obtained by quasi-elastic neutron scattering (QENS)[32,96,97]. Most models used to interpret QENS data treat a small portion of the pore water as immobile. In Fig. 8, we report the

average diffusion coefficient of all pore water (mobile or immobile) according to the models used to interpret QENS data. Takahara et al.[96] compared three different models for interpreting their QENS data in 2.14 and 2.84 nm diameter pores; in Fig. 8, we report their average estimates of D_{nanopore}. To account for the fact that the SPC/E model over-estimates the self-diffusion coefficient D_0 of bulk liquid water in systems larger than a few hundred water molecules, we report normalized pore diffusion coefficients D_{nanopore}/D_0, also known as steric constrictivity coefficients δ[98,99]. Overall, our MD simulations are remarkably consistent with the experimental results of Takahara et al.[31,96] and Matar Briman et al.[97] considering the non-triviality of the interpretation of QENS data[96,100] and the sensitivity of MD simulations to the choice of interatomic potential parameters. This sensitivity is illustrated in Fig. 8 by the MD simulation result of Lerbret et al.[37], who used a similar silanol density and the same SPC/E water model as this study but a different model of silica-water interactions. The blue curve in Fig. 8 shows the δ values that would be predicted by a conceptual model assigning zero mobility to water molecules in the first statistical water monolayer (within 3 Å of the silica surface) and full mobility to water located beyond the first layer. The success (even for pore diameters as low as 1 nm) of this very simple core-shell conceptual model is remarkable in view of the fact that the actual decrease in water mobility near hydrophilic surfaces occurs gradually over two or three water layers and that the first water layer is not really immobile[33-35,37,44] (Figs. 6-7).

Studies of bulk liquid water show that hydrogen bond breaking, an important step in water diffusion[101], occurs through discrete, large-amplitude rotations of a single water molecule that rapidly reorients a OH bond towards a new neighboring O atom[102]. This

rapid change in hydrogen bonding is preceded and facilitated by a slow (ps-scale) approach of the new neighbor O atom towards the reorienting water molecule[102]. In water-filled silica nanopores, this type of hydrogen bond breaking mechanism would be strongly inhibited in the first water layer by the fixed location of silanol groups and by steric constraints resulting from water density layering; hence, current understanding of hydrogen-bond breaking mechanisms is consistent with water diffusion being slowed down mostly in the first statistical water monolayer.

CONCLUSIONS

We find that silica surfaces carry up to three statistical monolayers of density-layered water. Bulk-liquid-like water (defined here as water with no density layering and with the same average density as bulk liquid water) exists in silica nanopores with diameters of 2 or 4 nm, but not in silica nanopores with diameters of 1 nm, in agreement with studies[2] that detected this transition at pore widths near 2 nm. The structural properties of interfacial water probed here (water density layering, water hydrogen bonding with silanol O atoms) are essentially identical in 2 and 4 nm nanopores and on flat silica surfaces, indicating that confinement and interfacial curvature do not significantly influence surface water structure as long as bulk-liquid-like water exists at the center of the pore. In 1 nm diameter pores, confinement (or curvature) strongly influences certain structural features (density layering) but not others (water hydrogen bonding with silanol O atoms). Our finding that water located at the center of 2 and 4 nm diameter pores has the same density as bulk liquid water contradicts the assumptions of several neutron diffraction[3,31] and MD simulation studies[38,43], but it supports recent MD simulation

results by Lerbret et al.[37]. Our results on water diffusion are consistent with QENS data[32,96,97] (yielding a measure of confidence in the quality of our MD simulations) and can be described with a very simple "core-shell" conceptual model on which the first water monolayer is immobile on diffusive time scales while the rest of the pore water diffuses as fast as bulk liquid water.

ACKNOWLEDGEMENT

This research was performed under the auspices of the Nuclear Energy Advanced Modeling and Simulation (NEAMS) program and was supported by the U.S. Department of Energy, Office of Nuclear Energy, under Contract No. DE-AC02-05CH11231. The quality of this manuscript was improved by comments from Benjamin Gilbert (LBNL) and from two anonymous reviewers.

SUPPORTING INFORMATION

Details of our simulations are described in the Electronic Annex. This information is available free of charge via the Internet at http://pubs.acs.org.

REFERENCES

(1) Alba-Simionesco, C.; Coasne, B.; Dosseh, G.; Dudziak, G.; Gubbins, K.E.; Radhakrishnan, R.; Sliwinska-Bartkowiak, M. *J. Phys.: Condens. Matter* **2006**, *18*, R15-R68.

(2) Mamontov, E.; Cole, D.R.; Dai, S.; Pawel, M.D.; Liang, C.D.; Jenkins, T.; Gasparovic, G.; Kintzel, E. *Chem. Phys.* **2008**, *352*, 117-124.

(3) Mancinelli, R.; Bruni, F.; Ricci, M.A. *J. Mol. Liq.* **2011**, *159,* 42-46.

(4) Le Caër, S.; Pin, S.; Esnouf, S.; Raffy, Q.; Renault, J.Ph.; Brubach, J.-B.; Creff, G.; Roy, P. *Phys. Chem. Chem. Phys.* **2011**, *13*, 17658-17666.

(5) Campen, R.K.; Pymer, A.K.; Nihonyanagi, S.; Borguet, E. *J. Phys. Chem. C* **2010**, *114*, 18465-18473.

(6) Jelassi, J.; Grosz, T.; Bako, I.; Bellissent-Funel, M.-C.; Dore, J.C.; Castricum, H.L.; Sridi-Dorbez, R. *J. Chem. Phys.* **2011**, *134*, 064509.

(7) Tilocca, A.; Cormack, A.N. *Proc. R. Soc. A* **2011**, *467*, 2102-2111.

(8) Cailleteau, C.; Devreux, F.; Spalla, O.; Angeli, F.; Gin, S. *J. Phys. Chem. C* **2011**, *115*, 5846-5855.

(9) Daval, D.; Sissmann, O.; Menguy, N.; Saldi, G.D.; Guyot, F.; Martinez, I.; Corvisier, J.; Garcia, B.; Machouk, I.; Knauss, K.G.; Hellmann, R. *Chem. Geol.* **2011**, *284*, 193-209.

(10) Navarre-Stichler, A.; Steefel, C.I.; Sak, P.B.; Brantley, S.L. *Geochim. Cosmochim. Acta* **2011**, *75*, 7644-7667.

(11) Loucaides, S.; Behrends, T.; Van Cappellen, P. *Geochim. Cosmochim. Acta* **2010**, *74*, 517-530.

(12) Gaus, I. *Int. J. Greenhouse Gas Control* **2010**, *4*, 73-89.

(13) Liu, F.; Lu, P.; Zhu, C.; Xiao, Y. *Int. J. Greenhouse Gas Control* **2011**, *5*, 294-307.

(14) Frugier, P.; Gin, S.; Minet, Y.; Chave, T.; Bonin, B.; Godon, N.; Lartigue, J.-E.; Jollivet, P.; Ayral, A.; De Windt, L.; Santarini, G. *J. Nucl. Mater.* **2008**, *380*, 8-21.

(15) Gin, S.; Guittonneau, C.; Godon, N.; Neff, D.; Rebiscoul, D.; Cabié, M.; Mostefaoui, S. *J. Phys. Chem. C* **2011**, *115*, 18696-18706.

(16) Goettmann, F.; Sanchez, C. *J. Mater. Chem.* **2007**, *17*, 24.

(17) Guégan, R. *J. Colloid Interface Sci.* **2011**, *358*, 485-490.

(18) Skinner, J.L.; Pieniazek, P.A.; Gruenbaum, S.M. *Acc. Chem. Res.* **2012**, *45*, 93-100.

(19) Schoch, R.B.; Han, J.; Renaud, P. *Rev. Mod. Phys.* **2008**, *80*, 839-883.

(20) Bocquet, L.; Charlaix, E. *Chem. Soc. Rev.* **2010**, *39*, 1073-1095.

(21) Hofmann, D.W.M.; Kuleshova, L.; D'Aguanno, B.; Di Noto, V.; Negro, E.; Conti, F.; Vittadello, M. *J. Phys. Chem. B* **2009**, *113*, 632-639.

(22) Alcantar, N.; Israelachvili, J.; Boles, J. *Geochim. Cosmochim. Acta* **2003**, *67*, 1289-1304.

(23) Bourg, I.C.; Sposito, G. *Environ. Sci. Technol.* **2010**, *44*, 2085-2091.

(24) Schreiber, A.; Ketelsen, I.; Findenegg, G.H. *Phys. Chem. Chem. Phys.*, **2001**, *3*, 1185-1195.

(25) Gruener, S.; Hofmann, T.; Wallacher, D.; Kityk, A.V.; Huber, P. *Phys. Rev. E* **2009**, *79*, 067301.

(26) Li, T.-D.; Gao, J.; Szoszkiewicz, R.; Landman, U.; Riedo, E. *Phys. Rev. B* **2007**, *75*, 115415.

(27) Brubach, J.-B.; Mermet, A.; Filabozzi, A.; Gerschel, A.; Lairez, D.; Krafft, M.P.; Roy, P. *J. Phys. Chem. B* **2001**, *105*, 430-435.

(28) Hansen, E.W.; Stöcker, M.; Schmidt, R. *J. Phys. Chem.* **1996**, *100*, 2195-2200.

(29) Morishige, K.; Nobuoka, K. *J. Chem. Phys.* **1997**, *107*, 6965-6969.

(30) Smirnov, P.; Yamaguchi, T.; Kittaka, S.; Takahara, S.; Kuroda, Y. *J. Phys. Chem. B* **2000**, *104*, 5498-5504.

(31) Thompson, H.; Soper, A.K.; Ricci, M.A.; Bruni, F.; Skipper, N.T. *J. Phys. Chem. B* **2007**, *111*, 5610-5620.

(32) Takahara, S.; Nakano, M.; Kittaka, S.; Kuroda, Y.; Mori, T.; Hamano, H.; Yamaguchi, T. *J. Phys. Chem. B* **1999**, *103*, 5814-5819.

(33) Castrillón, S.R.-V.; Giovambattista, N.; Aksay, I.A.; Debenedetti, P.G. *J. Phys. Chem. B* **2009**, *113*, 7973-7976.

(34) Kerisit, S.; Liu, C. *Environ. Sci. Technol.* **2009**, *43*, 777-782.

(35) Bourg, I.C.; Sposito, G. *J. Colloid Interface Sci.* **2011**, *360*, 701-715.

(36) Botan, A.; Rotenberg, B.; Marry, V.; Turq, P.; Noetinger, B. *J. Phys. Chem. C* **2011**, *115*, 16109-16115.

(37) Lerbret, A.; Lelong, G.; Mason, P.E.; Saboungi, M-L.; Brady, J.W. *Food Biophys.* **2011**, *6*, 233-240.

(38) Gallo, P.; Rovere, M.; Spohr, E. *J. Chem. Phys.* **2000**, *113*, 11324-11335.

(39) Joseph, S.; Aluru, N.R. *Langmuir* **2006**, *22*, 9041-9051.

(40) Leung, K.; Rempe, S.B.; Lorenz, D. *Phys. Rev. Lett.* **2006**, *96*, 095504.

(41) Cruz-Chu, E.R.; Aksimentiev, A.; Schulten, K. *J. Phys. Chem. B* **2006**, *110*, 21497-21508.

(42) Cruz-Chu, E.R.; Aksimentiev, A.; Schulten, K. *J. Phys. Chem. C* **2009**, *113*, 1850-1862.

(43) Milischuk, A.A.; Ladanyi, B.M. *J. Chem. Phys.* **2011**, *135*, 174709.

(44) Siboulet, B.; Coasne, B.; Dufrêche, J.-F.; Turq, P. *J. Phys. Chem. B* **2011**, *115*, 7881-7886.

(45) Ho, T.A.; Argyris, D.; Cole, D.R.; Striolo, A. *Langmuir* **2012**, *28*, 1256-1266.

(46) Guégan, R.; Morineau, D.; Alba-Simionesco, C. *Chem. Phys.* **2005**, *317*, 236-244.

(47) Zhuravlev, L.T. *Colloids Surf. A* **2000**, *173*, 1-38.

(48) Plimpton, S. *J. Comput. Phys.* **1995**, *117*, 1-42.

(49) Humphrey, W.; Dalke, A.; Schulten, K. *J. Molec. Graphics* **1996**, *14*, 33-38.

(50) Skelton, A.A.; Fenter, P.; Kubicki, J.D.; Wesolowski, D.J.; Cummings, P.T. *J. Phys. Chem. C* **2011**, *115*, 2076-2088.

(51) Lee, S.H.; Rossky, P.J. *J. Chem. Phys.* **1994**, *100*, 3334-3345.

(52) Rustad, J.R.; Hay, B.P. *Geochim. Cosmochim. Acta* **1995**, *59*, 1251-1257.

(53) Rovere, M.; Ricci, M.A.; Vellati, D.; Bruni, F. *J. Chem. Phys.* **1998**, *108*, 9859-9867.

(54) Puibasset, J.; Pellenq, R.J.-M. *J. Chem. Phys.* **2003**, *118*, 5613-5622.

(55) Cygan, R.T.; Liang, J.-J.; Kalinichev, A.G. *J. Phys. Chem. B* **2004**, *108*, 1255-1266.

(56) Lopes, P.E.M.; Murashov, V.; Tazi, M.; Demchuk, E.; MacKerell, A.D., Jr. *J. Phys. Chem. B* **2006**, *110*, 2782-2792.

(57) Lockwood, G.K.; Garofalini, S.H. *J. Chem. Phys.* **2009**, *131*, 074703.

(58) Fogarty, J.C.; Aktulga, H.M.; Grama, A.Y., van Duin, A.C.T.; Pandit, S.A. *J. Chem. Phys.* **2010**, *132*, 174704.

(59) Hassanali, A.A.; Singer, S.J. *J. Phys. Chem. B* **2007**, *111*, 11181-11193.

(60) Shirono, K.; Tatsumi, N.; Daiguji, H. *J. Phys. Chem. B* **2009**, *113*, 1041-1047.

(61) Ohno, H.; Kohara, S.; Umesaki, N.; Suzuya, K. *J. Non-Cryst. Solids* **2001**, *293-295*, 125-135.

(62) Schlegel, M.L.; Nagy, K.L.; Fenter, P.; Sturchio, N.C. *Geochim. Cosmochim. Acta* **2002**, *66*, 3037-3054.

(63) Hudon, P.; Jung, I.-H.; Baker, D.R. *Phys. Earth Planet. Int.* **2002**, *130*, 159-174.

(64) Berendsen, H.J.C.; Grigera, J.R.; Straatsma, T.P. *J. Phys. Chem.* **1987**, *91*, 6269-6271.

(65) Smith, D.E.; Dang, L.X. *J. Chem. Phys.* **1994**, *100*, 3757-3766.

(66) Wasserman, E.; Wood, B.; Brodholt, J. *Geochim. Cosmochim. Acta* **1995**, *59*, 1-6.

(67) Hura, G.; Russo, D.; Glaeser, R.M.; Head-Gordon, T.; Krack, M.; Parrinello, M. *Phys. Chem. Chem. Phys.* **2003**, *5*, 1981-1991.

(68) Ferrage, E.; Sakharov, B.A.; Michot, L.J.; Delville, A.; Bauer, A.; Lanson, B.; Grangeon, S.; Frapper, G.; Jiménez-Ruiz, M.; Cuello, G.J. *J. Phys. Chem. C* **2011**, *115*, 1867-1881.

(69) Marry, V.; Dubois, E.; Malikova, N.; Durand-Vidal, S.; Longeville, S.; Breu, J. *Environ. Sci. Technol.* **2011**, *45*, 2850-2855.

(70) Toney, M.F.; Howard, J.N.; Richer, J.; Borges, G.L.; Gordon, J.G.; Melroy, O.R.; Wiesler, D.G.; Yee, D.; Sorensen, L.B. *Surf. Sci.* **1995**, *335*, 326-332.

(71) Benham, M.J.; Cook, J.C.; Li, J.-C.; Ross, D.K.; Hall, P.L.; Sarkissian, B. *Phys. Rev. B* **1989**, *39*, 633-636.

(72) Bickmore, B.R.; Wheeler, J.C.; Bates, B.; Nagy, K.L.; Eggett, D.L. *Geochim. Cosmochim. Acta* **2008**, *72*, 4521-4536.

(73) Carroll, S.A.; Maxwell, R.S.; Bourcier, W.; Martin, S.; Hulsey, S. *Geochim. Cosmochim. Acta* **2002**, *66*, 913-926.

(74) Wang, M.; Revil, A. *J. Colloid Interface Sci.* **2010**, *343*, 381-386.

(75) Andersen, M.B.; Bruus, H.; Bardhan, J.P.; Pennathur, S. *J. Colloid Interface Sci.* **2011**, *360*, 262-271.

(76) Hiemstra, T.; Venema, P.; Van Riemsdijk, W.H. *J. Colloid Interface Sci.* **1996**, *184*, 680-692.

(77) Bickmore, B.R.; Tadanier, C.J.; Rosso, K.M.; Monn, W.D.; Eggett, D.L. *Geochim. Cosmochim. Acta* **2004**, *68*, 2025-2042.

(78) Machesky, M.L.; Predota, M.; Wesolowski, D.J.; Vlcek, L.; Cummings, P.T.; Rosenqvist, J.; Ridley, M.K.; Kubicki, J.D.; Bandura, A.V.; Kumar, N.; Sofo, J.O. *Langmuir* **2008**, *24*, 12331-12339.

(79) Fernández-Martínez, A. **2009**. Ph.D. thesis, U. of Grenoble.

(80) McGrail, B.P.; Icenhower, J.P.; Shuh, D.K.; Liu, P.; Darab, J.G.; Baer, D.R.; Thevuthasen, S.; Shutthanandan, V.; Engelhard, M.H.; Booth, C.H.; Nachimuthu, P. *J. Non-Cryst. Solids* **2001**, *296*, 10-26.

(81) Leung, K.; Nielsen, I.M.B.; Criscenti, L.J. *J. Am. Chem. Soc.* **2009**, *131*, 18358-18365.

(82) Sonnefeld, J.; Löbbus, M.; Vogelsberger, W. *Colloids Surf. A* **2001**, *195*, 215-225.

(83) Dove, P.M.; Craven, C.M. *Geochim. Cosmochim. Acta* **2005**, *69*, 4963-4970.

(84) Sverjensky, D.A.; Sahai, N. *Geochim. Cosmochim. Acta* **1996**, *60*, 3773-3797.

(85) Sulpizi, M.; Gaigeot, M.-P.; Sprik, M. *J. Chem. Theory Comput.* **2012**, *8*, 1037-1047.

(86) Rotenberg, B.; Marry, V.; Vuilleumier, R.; Malikova, N.; Simon, C.; Turq, P., *Geochim. Cosmochim. Acta* **2007**, *71*, 5089-5101.

(87) Churakov, S.V.; Gimmi, T. *J. Phys. Chem. C* **2011**, *115*, 6703-6714.

(88) Renkin, E.M. *J. Gen. Physiol.* **1954**, *38*, 225-243.

(89) Deen, W.M. *AIChE J.* **1987**, *33*, 1409-1425.

(90) Prakash, S.; Piruska, A.; Gatimu, E.N.; Bohn, P.W.; Sweedler, J.V.; Shannon, M.A. *IEEE Sensors J.* **2008**, *8*, 441-450.

(91) Wernert, V.; Bouchet, R.; Denoyel, R. *Micropor. Mesopor. Mat.* **2011**, *140*, 97-102.

(92) Liu, P.; Harder, E.; Berne B.J. *J. Phys. Chem. B* **2004**, *108*, 6595-6602.

(93) Yeh, I.-C.; Hummer, G. *J. Phys. Chem. B* **2004**, *108*, 15873-15879.

(94) Kerisit, S.; Liu, C. *Geochim. Cosmochim. Acta* **2010**, *74*, 4937-4952.

(95) Mills, R. *J. Phys. Chem.* **1973**, *77*, 685-688.

(96) Takahara, S.; Sumiyama, N.; Kittaka, S.; Yamaguchi, T.; Bellissent-Funel, M.-C. *J. Phys. Chem. B* **2005**, *109*, 11231-11239.

(97) Matar Briman, I.; Rébiscoul D.; Diat O.; Zanotti, J.-M.; Jollivet, P.; Barboux, P.; Gin, S. *J. Phys. Chem. C* **2012**, *116*, 7021-7028.

(98) Boving, T.B.; Grathwohl, P. *J. Contam. Hydrol.* **2001**, *53*, 85-100.

(99) Bourg, I.C.; Sposito, G.; Bourg, A.C.M. *Clays Clay Miner.* **2006**, *54*, 363-374.

(100) Marry, V.; Malikova, N.; Cadène, A.; Dubois, E.; Durand-Vidal, S.; Turq, P.; Breu, J.; Longeville, S.; Zanotti, J.-M. *J. Phys.: Condens. Matter* **2008**, *20*, 104205.

(101) Agmon, N. *Acc. Chem. Res.* **2012**, *45*, 63-73.

(102) Laage, D.; Stirnemann, G.; Sterpone, F.; Hynes, J.T. *Acc. Chem. Res.* **2012**, *45*, 53-62.

(103) Kihara, K. *Eur. J. Mineral.* **1990**, *2*, 63-77.

(104) Jorgensen, W.L.; Chandrasekhar, J.; Madura, J.D.; Impey, R.W.; Klein, M.L. *J. Chem. Phys.* **1983**, *79*, 926-935.

(105) Lynden-Bell, R.M.; Rasaiah, J.C. *J. Chem. Phys.* **1996**, *105*, 9266-9280.

(106) Yang, Y.; Henderson, D.; Crozier, P.; Rowley, R.L.; Busath, D.D. *Mol. Phys.* **2002**, *100*, 3011-3019.

Table 1. SiO_2 glass structure (density and radial distribution function peak coordinates) at 298 K predicted with the LR[51], CLAYFF[55], LRL[40], and JA[39] models (this study), by the REAXFF model[58], and measured by neutron diffraction[61]. Confidence intervals on the radial distribution function peak coordinates are approximately ± 0.01 Å.

Model	Density (kg dm^{-3})	Si-O first max. (Å)	O-O first max. (Å)	Si-Si first max. (Å)	Si-O second max. (Å)
LRL	0.51	3.07	3.57	4.18	6.25
JA	0.65	2.93	3.37	4.69	5.97
LR	1.03	2.97	3.47	4.79	6.13
CLAYFF	2.15	1.57	2.55	3.11	3.99
REAXFF[a]	2.14	1.56	2.53	3.06	3.90
Experiment[b]	2.20	1.60	2.61	3.115	4.13

[a]Calculated by Fogarty et al.[58].

[b]Radial distribution function peak positions were read from the neutron diffraction results of Ohno et al.[61]; density was reported by Hudon et al.[63].

Figure 1. Molecular dynamics simulation snapshots of 6-Å-thick cross-sections [normal (left) or parallel (right) to the pore axis] of the 4 nm diameter pore (yellow, red, and white: Si, O, and H atoms in the silica structure; dark and light blue: water O and H atoms). Silanol OH groups are highlighted as red and white spheres in the cross-section on the left-hand-side. The 4-nm-thick water films that cover both surfaces of the silica slab are visible in the cross-section on the right-hand-side. The simulation cell (63.29126 × 73.08256 × 190.0 Å) includes a 5-nm-thick vapor gap between periodic images in the *z* direction (normal to the silica slab).

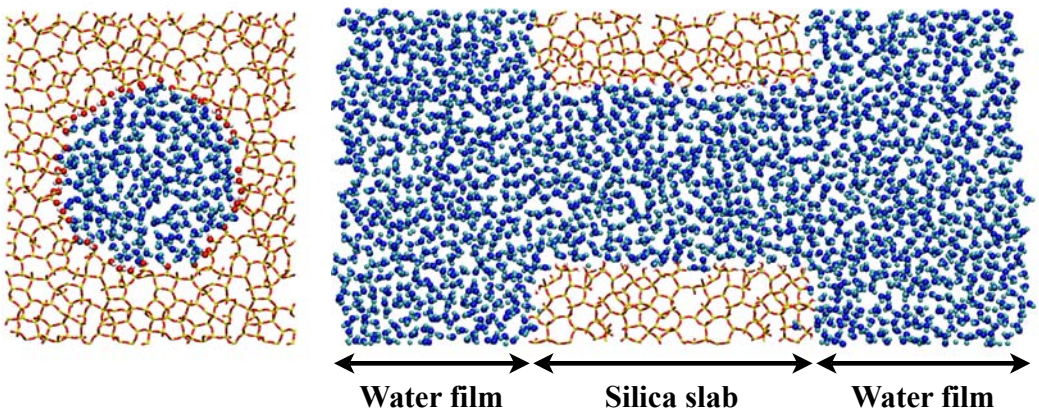

Figure 2. Average density of water O atoms (ρ_{Ow}) in 1, 2, and 4 nm diameter pores (from top to bottom) plotted as a function of *z* (horizontal axis) and distance *r* from the pore axis (vertical axis). Red color indicates ρ_{Ow} values greater than the average O atom density in the bulk liquid. Water density layering occurs within about 1 nm of the silica surfaces.

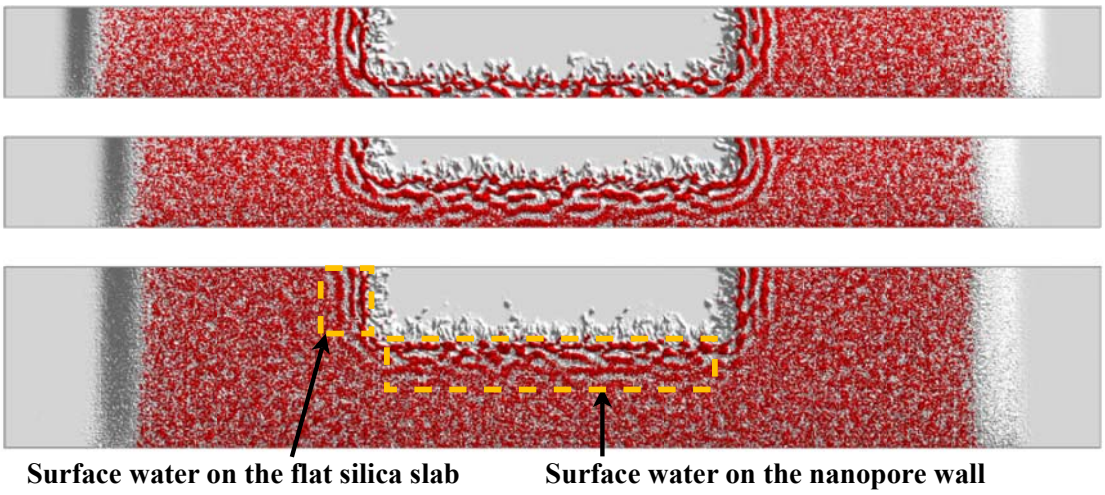

Figure 3. (a) Average density of silanol H (in black), Ow (in red), and Hw atoms (in blue) as a function of distance from the curved surface of the 2 nm diameter pore, calculated for z = 75 to 115 Å. (b) Comparison of the average Ow density (ρ_{Ow}) profiles on flat surfaces (calculated for r = 23.0 to 31.2 Å in the 4 nm diameter pore simulations) and on curved nanopore surfaces (z = 75 to 115 Å). (c) Same as Fig. 3b for ρ_{Hw}.

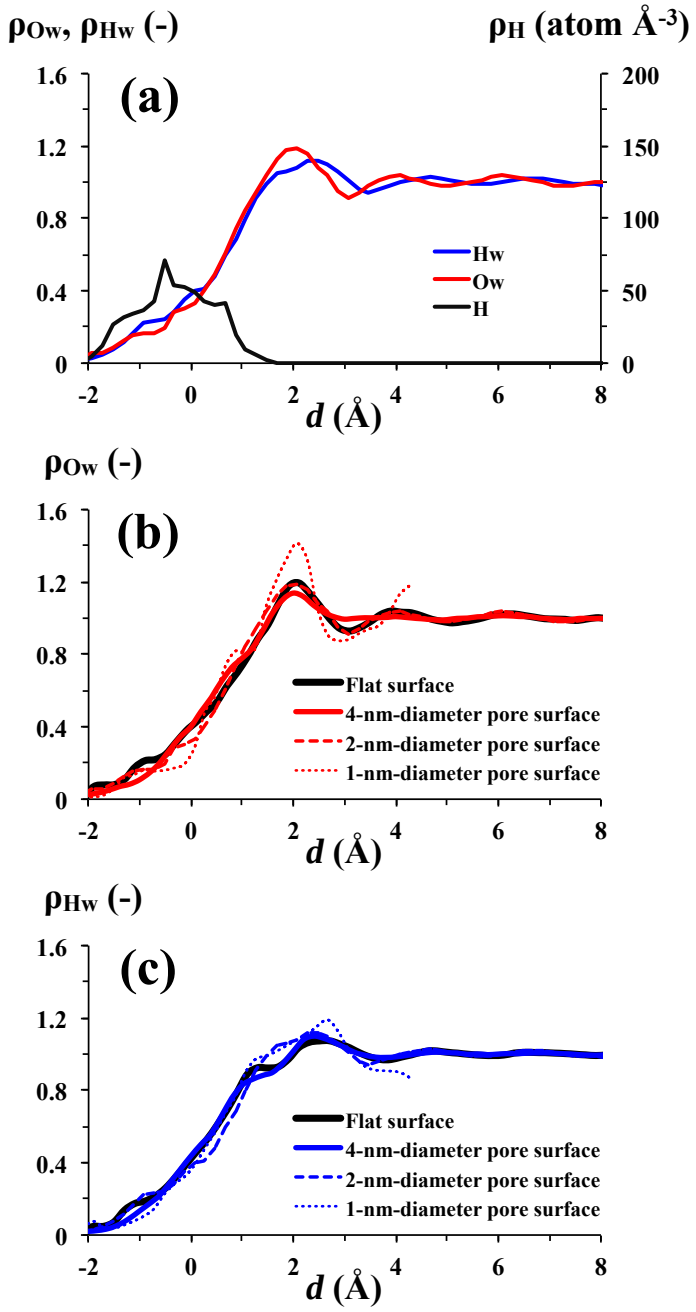

Figure 4. Cumulative distribution of the $s_{H\text{-}bond}$ values (in valence units) of silanol sites located on flat surfaces (r > 22 in the 4 nm diameter nanopore simulation) and on curved nanopore surfaces (z = 67 to 123 Å).

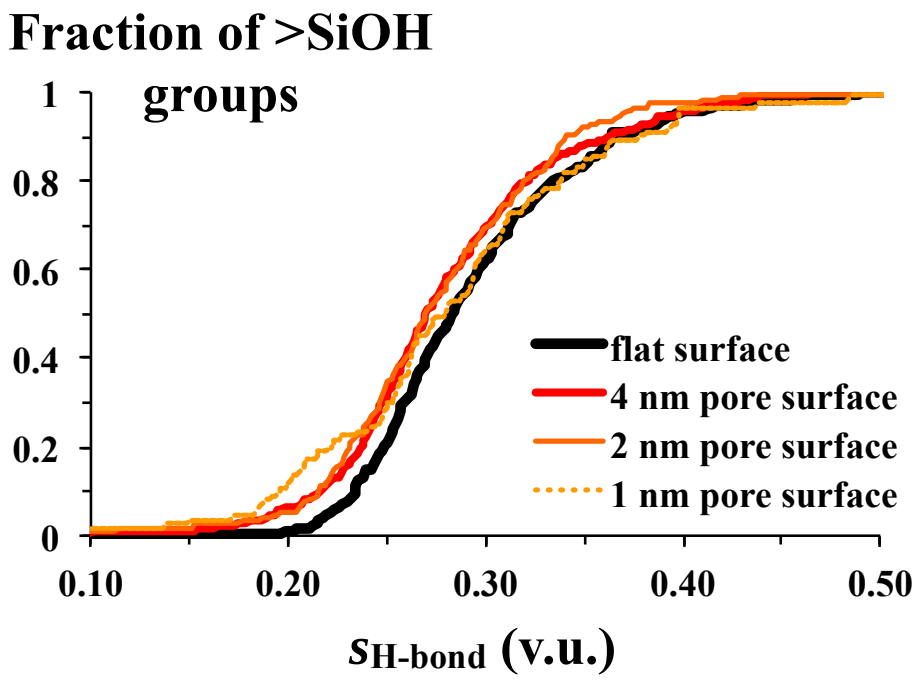

Figure 5. Upper graph: average density distribution of "tagged" water O atoms (normalized to the average density of water O atoms, averaged over both *z* directions, and plotted as a function of *z*) during several time intervals after the beginning of the 2 nm diameter nanopore simulation. Lower graph: cumulative breakthrough flux of tagged water O atoms diffusing through 1, 2, and 4 nm diameter nanopores (averaged over both directions, normalized to pore cross-section area) plotted as a function of time since the beginning of the MD simulation.

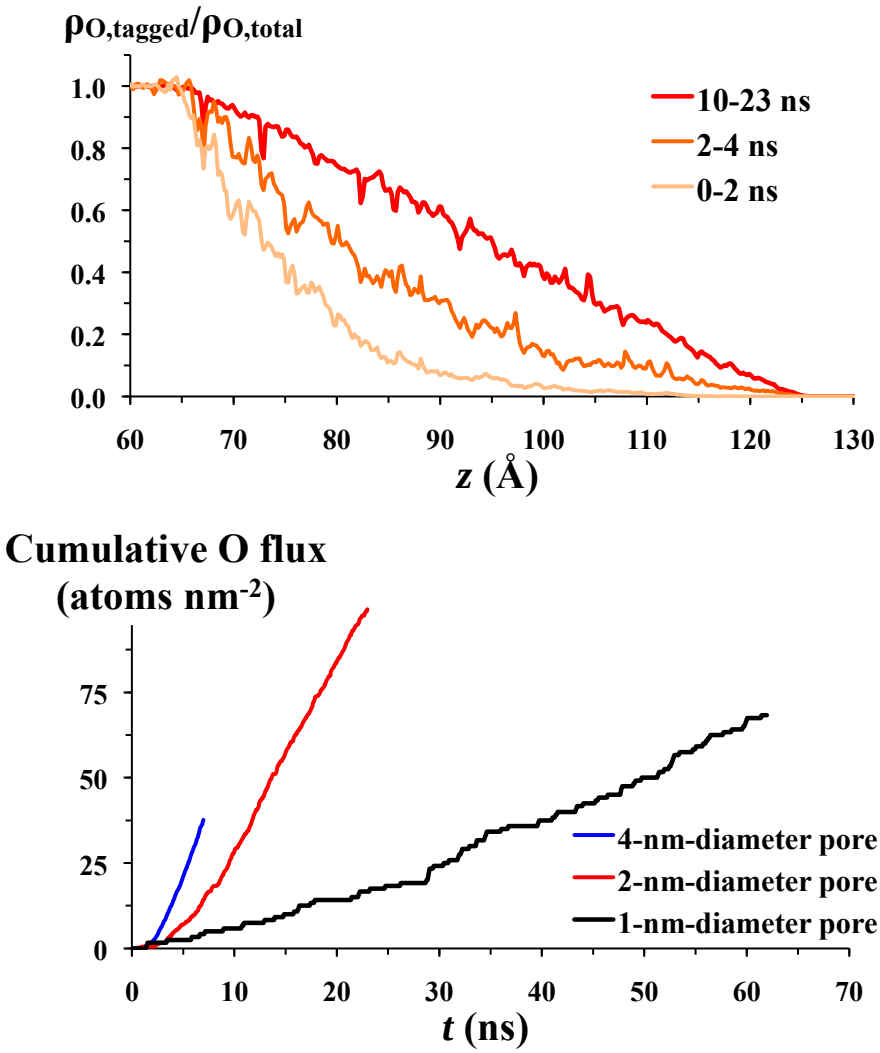

Figure 6. Molecular scale diffusion coefficient of water molecules, calculated from the mean-square-displacement of water O atoms during 10 ps, plotted as a function of *z* (horizontal axis) and distance *r* from the pore axis (vertical axis) in the 1, 2, and 4 nm diameter pores.

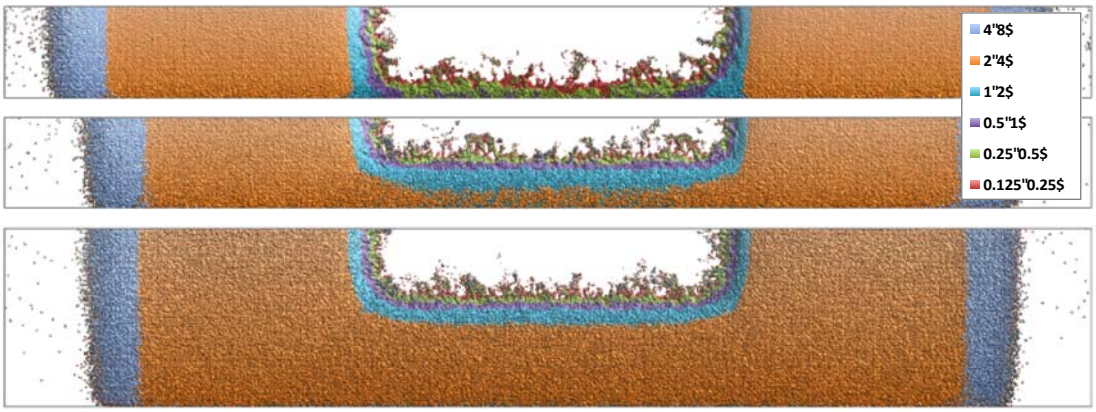

Figure 7. Molecular scale diffusion coefficient of water molecules, plotted as a function of distance from the silica surface, on flat surfaces (region where r = 23.0 to 31.2 Å in the 4 nm diameter pore simulations) and on curved nanopore surfaces (z = 75 to 115 Å).

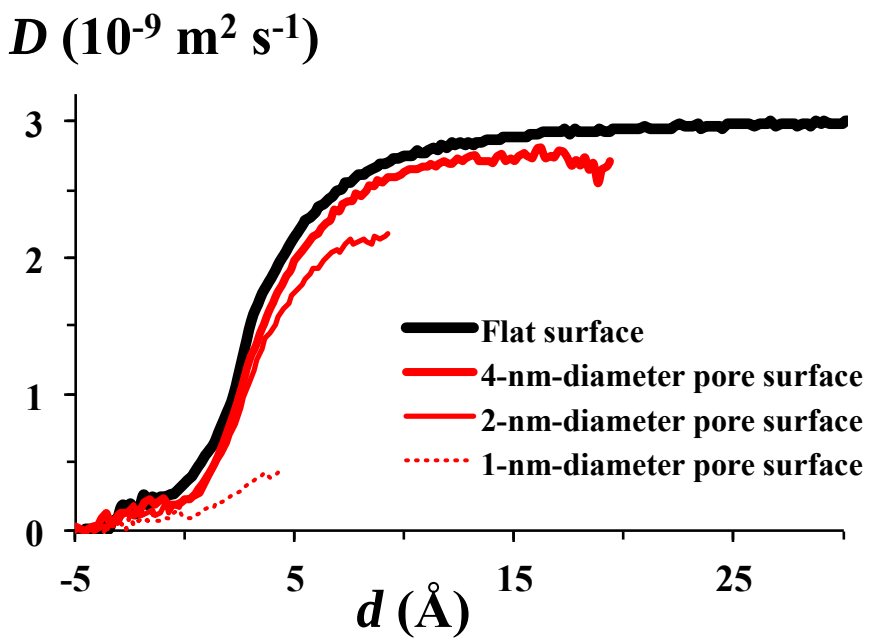

Figure 8. Pore scale water diffusion coefficient in silica nanopores, normalized to the self-diffusion coefficient of bulk liquid water ($\delta = D_{nanopore}/D_0$), plotted as a function of pore diameter at 298 K (most data) or 300 K[32]. Error bars (95 % confidence intervals) on the data of Takahara et al.[96] were calculated as two standard errors of the mean, treating their three data analysis methods as a "replicates" of the same measurement. Error bars on the data of Takahara et al.[32] were estimated using the standard error calculated from the data of Takahara et al.[96]. The data of Matar Briman et al.[97] were converted to $D_{nanopore}$ values by assuming that the fraction of immobile water in their pores was roughly 0.8 times the fraction of immobile protons (as suggested by the data of Takahara et al.[32]). We used $D_0 = 2.299 \times 10^{-9}$ m^2 s^{-1} for real water at 298 K[95], $D_0 = 2.41 \times 10^{-9}$ m^2 s^{-1} for real water at 300 K (interpolated from D_0 values at 298 and 308 K[95] using an Arrhenius relation), and $D_0 = 2.84 \pm 0.2 \times 10^{-9}$ m^2 s^{-1} for SPC/E water at 298 K[94] (with a confidence interval roughly estimated from the data of Kerisit et al.[94]). The line shows the trend that would be predicted by a very simple "core-shell" conceptual model assigning zero mobility to water molecules in the first statistical water monolayer and full mobility to water located beyond the first layer.

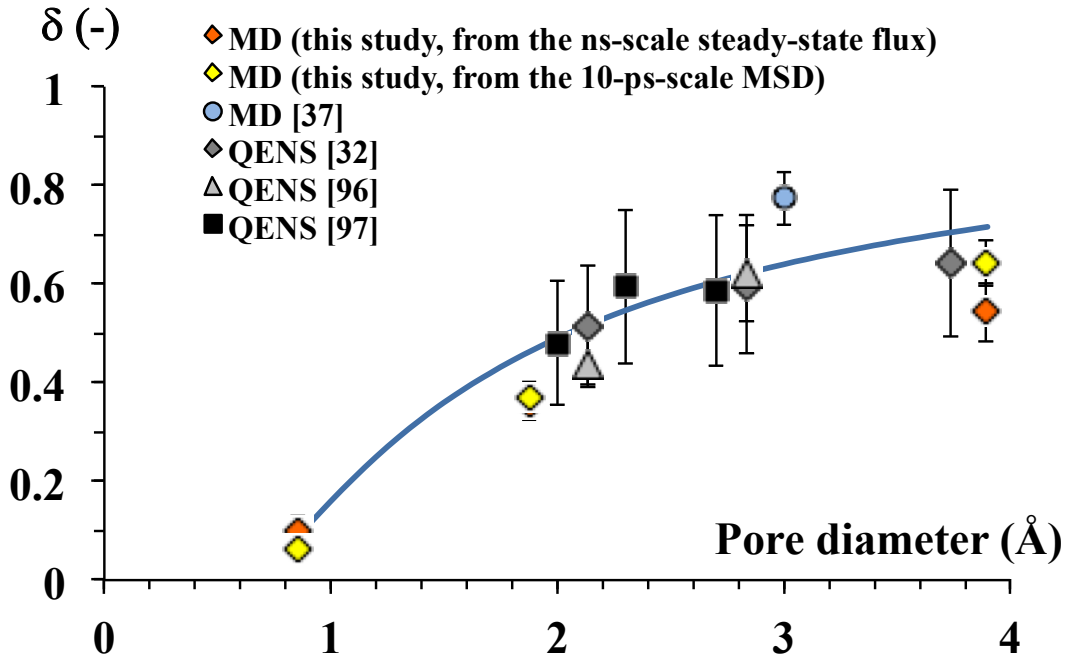

ELECTRONIC ANNEX

SiO_2 glass structure test simulations. For our first test of SiO_2-water interaction models, we applied a series of annealing cycles to a 29.4822 × 34.0431 × 32.4282 Å simulation cell containing 288 unit cells of α-quartz (total 2592 atoms) constructed with the atomic coordinates of Kihara[103]. Each cycle consisted of 1 ns of equilibration at the annealing temperature T_{anneal} (NPT ensemble; P = 0 MPa; thermostat and barostat coupling constants of 10 and 50 ps), quenching to 298 K at the rate of 2 K ps^{-1} (same pressure and thermo-/barostat coupling constants), 1 ns of equilibration at 298 K (same pressure; thermostat and barostat coupling constants of 100 and 1000 ps), and 1 ns of equilibration at 298 K (NVT ensemble; thermostat coupling constant of 100 ps). Selected simulation times and quenching rates are typical of silicate melt simulations[41]. Successive annealing cycles were carried out for increasing T_{anneal} values until the SiO_2 fluid "vaporized" (i.e., density dropped below 0.2 kg dm^{-3}) or until T_{anneal} = 5000 K. Radial distribution functions g_{SiSi}, g_{SiO} and g_{OO} of quenched SiO_2 glasses were acquired during the last 100 ps of each annealing cycle; coordinates of the first peaks of these functions and SiO_2 glass densities are reported in Table 1 along with experimental data[61] and MD simulation results obtained by Fogarty et al.[58] with the reactive force field REAXFF. The CLAYFF model of Cygan et al.[55] performed much better than other two-body interaction models (Table 1); in fact, it predicted radial distribution function peak coordinates slightly more accurately than the much more complex REAXFF model of Fogarty et al.[58].

To test the influence of quenching rate on the structure of SiO_2 glass, we repeated our simulation with the CLAYFF model using a slower quenching rate (0.4 K ps^{-1}). This

yielded no significant difference in bulk density or radial distribution function peak coordinates, but it decreased the density of structural defects (the fraction of non-bridging O atoms decreased from 0.52 to 0.29 %).

Quartz-water interface test simulations. For our second test, we cleaved a α-quartz crystal along "termination β" of the $10\bar{1}0$ face[62] to create a 29.4822 × 32.4282 × 37 Å slab (periodic in the *x* and *y* dimensions). We placed this slab in a 29.4822 × 32.4282 × 140 Å periodically replicated simulation cell. Then, we healed both $10\bar{1}0$ surfaces with H atoms placed 1 Å directly above each under-coordinated surface O atom. Finally, we placed a 6-nm-thick water film (1900 water molecules) on one of the two $10\bar{1}0$ surfaces of our quartz slab. Our interest being in the structure and diffusion of water at 298 K, we carried out all test simulations using the SPC/E water model[64], which accurately describes the structure[67], diffusion coefficient (in simulations of a few hundred water molecules[65]), and static dielectric constant[66] of ambient liquid water. The SPC/E water model was used in the original implementation of the LRL[40] and JA[39] silica-water interaction models and is frequently used with the CLAYFF model[23,50,68,69], whereas the LR[51] silica-water interaction model was originally implemented with the TIP4P water model[104]. We simulated our quartz-water systems for 500 ps at 298 K with a 0.5 fs time step (after 502 ps of equilibration) with fixed atomic coordinates for quartz Si and O atoms. Simulation results on the distance between the plane of Si atoms closest to the interface and the first peak of water O atom density are shown in Table A2 along with the X-ray reflectivity measurement of Schlegel et al.[62]. Evidently, the adequacy of the four tested SiO_2-water models cannot be distinguished based on the experimental data of

Schlegel et al.[62]. In a recent study, however, Skelton et al.[50] showed that CLAYFF model is consistent with *ab initio* MD predictions of water structure on the $10\bar{1}1$ quartz surface.

Silica nanopore simulations. Our nanopores were constructed from SiO_2 glass as in previous studies[38,40,53]. We used a silica glass structure generated with the CLAYFF model to create a 29.4822 × 34.0431 × 64.8564 Å glass slab in a 29.4822 × 34.0431 × 190.0 Å simulation cell (the glass slab was centered at z = 95 Å). To create 1 or 2 nm diameter pores, we removed all Si atoms located within 0.5 or 1.0 nm of the pore axis as well as all Si atoms located at z < 65 or z > 125 Å. Then, we removed all O atoms that were not coordinated to at least one Si atom. Finally, we attached an H atom to each singly-coordinated O atom, with very few exceptions as required to maintain charge balance. Finally, we placed 2040 water molecules on each side of the silica slab. For our 4-nm-diameter pore, we replicated our glass slab in the x and y dimensions before removing all Si atoms located within 2.0 nm of the pore axis, and we placed 8160 water molecules on each side of the glass slab. During the equilibration period, water imbibed the nanopores, in agreement with the hydrophilic nature of hydroxylated silica surfaces[41]. Periodic boundary conditions have no discernible influence on the behavior of water and ions in cylindrical nanopores for systems as large as those simulated here[105,106]. To calculate the location of the Gibbs dividing surface of water on flat slab surfaces (z_G) and on curved pore walls (r_G), we used the standard relations:

$$\int_{z=z^*}^{z=z_G} \rho_{O_w}(z)\,\mathrm{d}z = \rho_{O_w,\mathrm{bulk}}(z_G - z^*)$$

where z^* is a z-coordinate sufficiently far from the flat slab surface that ρ_{Ow} has the uniform, bulk-liquid value $\rho_{Ow,bulk}$, and:

$$\int_{r=0}^{r=r_G} \rho_{O_w}(r)2r\,\mathrm{d}r = \rho_{O_w,\mathrm{bulk}}(r_G)^2 .$$

Table A1. Parameters of the SiO_2-water models considered in the present study. In these models, interatomic potentials are represented as the sum of a long-range Coulombic interaction between atoms of charge q_i (e) and a short-range Lennard-Jones 6-12 interaction potential $\phi_{ij}(r) = 4\varepsilon_{ij}\,[(\sigma_{ij}/r)^{12} - (\sigma_{ij}/r)^{6}]$, where r is the i-j interatomic distance, ϕ_{ij} is the short-range interaction potential, and $2^{1/6}\sigma_{ij}$ and ε_{ij} are the location (Å) and depth (kJ mol^{-1}) of the i-j potential well. Parameters σ_{ij} and ε_{ij} are obtained for any i-j atom pairs from the Lorentz-Berthelot combining rules [$\sigma_{ij} = ½(\sigma_i + \sigma_j)$ and $\varepsilon_{ij} = \varepsilon_i^{1/2}\varepsilon_j^{1/2}$]. The behavior of surface H atoms was constrained with a fixed Si-O-H angle and O-H bond length [LR model: 109.5° and 0.9572 Å; CLAYFF and JA models: 109.47° and 1.0 Å; LRL model: 120° and 0.968 Å; Si-O-H angles and O-H bond lengths were "stiffened" by setting harmonic bending and stretching constants to values ten times higher than in the original models or, if not defined, ten times higher than in the CLAYFF model].

Atom type	σ (Å)	ε (kJ mol^{-1})	q (e)
LR[51] *model*[a]			
Si	3.795	0.5336	1.24
O	3.154	0.6487	-0.62
Oh[b]	3.154	0.6487	-0.71
H	0	0	0.4
CLAYFF[55] *model*			
Si	3.30203	7.7005×10^{-6}	2.1
O	3.16556	0.65017	-1.05
Oh	3.16556	0.65017	-0.95
H	0	0	0.425
LRL[40] *model*[c]			
Si	4.0	0.41839	1.2
O	3.16556	0.65017	-0.6
Oh	3.16556	0.65017	-0.73
H	0	0	0.43
JA[39] *model*[d]			
Si	3.386	2.447	1.36
O	3.16556	0.65017	-0.68
Oh	3.16556	0.65017	-0.78
H	0	0	0.44

[a]Lee and Rossky[51] estimated q for surface Oh and H atoms, assigned q = 0 e to all non-silanol Si and O atoms, and deduced q = 0.31 e for silanol Si atoms. Instead, we used the same q values for Oh and H atoms and assumed that all Si atoms have identical q values, which yields q_{Si} = 1.24 e and q_O = -0.62 e.

[b]Silanol O atom.

[c]Leung et al.[40] used q_{Oh} = -0.74 e and adjusted each q_{Si} to yield local charge neutrality. For simplicity, we used q_{Si} = 1.2 e and q_{Oh} = -0.73 e.

[d]Joseph and Aluru[39] used the short-range interaction parameters of SPC/E water O atoms for silica O and Oh atoms, but they erroneously reported these as σ_O = 3.169 Å and ε_O = 0.6502 kJ mol^{-1}. We modified their q_{Oh} value from -0.77 to -0.78 e to ensure charge neutrality.

Table A2. Distance between the plane of Si atoms closest to the quartz surface and the first peak of the water O density profile on the $10\bar{1}0$ surface of α-quartz at 298 K predicted by the LR, CLAYFF, LRL, and JA models (this study) and measured by X-ray reflectivity[62].

Model	Si-water O distance (Å)
LR	3.46 ± 0.02
CLAYFF	3.48 ± 0.02
LRL	3.48 ± 0.02
JA	3.40 ± 0.02
Experiment	3.2 ± 0.1

Table of Contents – Graphic

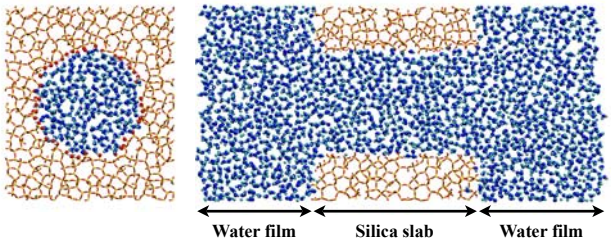

DISCLAIMER

This document was prepared as an account of work sponsored by the United States Government. While this document is believed to contain correct information, neither the United States Government nor any agency thereof, nor The Regents of the University of California, nor any of their employees, makes any warranty, express or implied, or assumes any legal responsibility for the accuracy, completeness, or usefulness of any information, apparatus, product, or process disclosed, or represents that its use would not infringe privately owned rights. Reference herein to any specific commercial product, process, or service by its trade name, trademark, manufacturer, or otherwise, does not necessarily constitute or imply its endorsement, recommendation, or favoring by the United States Government or any agency thereof, or The Regents of the University of California. The views and opinions of authors expressed herein do not necessarily state or reflect those of the United States Government or any agency thereof or The Regents of the University of California.

Ernest Orlando Lawrence Berkeley National Laboratory is an equal opportunity employer.